Wind survey of high-speed bulk flows and field-aligned beams in the near-Earth plasma sheet

Arjun Raj, Tai Phan, Robert P. Lin, and V. Angelopoulos
Space Sciences Laboratory, University of California at Berkeley, Berkeley, California, USA

Received 3 August 2001; revised 26 December 2001; accepted 15 April 2002; published 3 December 2002.

[1] We have surveyed all high-speed (>250 km/s) flows detected by Wind during its 17 perigee passes across the near-Earth ($x_{GSE} = -25$ to 0 R_E) plasma sheet in the period between 1995 and 1997. By classifying high-speed flow events based on their ion distribution characteristics rather than their plasma moments or the regions in which these flows were detected, we found that most (if not all) high-speed flow ion distributions fall into two distinct categories: bulk flows and field-aligned beams. We show that bulk flows are not simply the low-latitude counterparts of field-aligned beams. Field-aligned beams have sharp cutoffs at low energies, occur within relatively steady magnetic field and plasma conditions, and are detected more often away from the neutral sheet. On the other hand, high-speed bulk flows are well represented by a single drifting population and have their peak occurrence rate at the neutral sheet. Bulk flows are generally accompanied by large magnetic field fluctuations and sudden increase of energetic (up to 0.5 MeV) particle fluxes. They are often (but not always) associated with magnetic field dipolarization and plasma temperature enhancements. Little or no temperature enhancements are observed in cases where the spacecraft resides near the neutral sheet before the arrival of bursty bulk flows, suggesting that temperature enhancements seen in other bulk flow events may in part be a spatial effect instead of true heating of the plasma. Bulk flows are perpendicular to the magnetic field when detected at the neutral sheet but have a large field-aligned component at higher magnetic latitudes. Field-aligned bulk flows and field-aligned beams are similar in terms of their velocity moments and may occur at the same magnetic latitudes but are easily distinguishable based on their ion distributions. We have used our categorization of bulk flow and field-aligned beam events to search for the optimal moment-based selection criteria to distinguish bulk flows from beams. We found that no single moment-based parameter or threshold can serve to cleanly separate beam from bulk flow distributions because a range of values of these parameters exists where both types of fast flows are observed. We found perpendicular flow speed $v_\perp > 250$ km/s and plasma β_{xy} (based on the x and y components of the magnetic field) > 2 to be the optimal moment-based bulk flow selection criteria because they eliminate ~95% of beam events while retaining ~60% of bulk flow events. Finally, a previously reported dawn–dusk asymmetry in the occurrence of bursty bulk flows, with most events occurring in the premidnight sector, is confirmed by our survey. Field-aligned beams, on the other hand, have no dawn–dusk bias. *INDEX TERMS:* 2744 Magnetospheric Physics: Magnetotail; 2764 Magnetospheric Physics: Plasma sheet; 2788 Magnetospheric Physics: Storms and substorms; *KEYWORDS:* bursty bulk flow, PSBL beams, BBF selection criteria, dawn-dusk asymmetry

Citation: Raj, A., T. Phan, R. P. Lin, and V. Angelopoulos, Wind survey of high-speed bulk flows and field-aligned beams in the near-Earth plasma sheet, *J. Geophys. Res.*, *107*(A12), 1419, doi:10.1029/2001JA007547, 2002.

1. Introduction

[2] The existence of high-speed plasma flows in the near-Earth plasma sheet has been well established for some time. The fast "flows" observed at the high-latitude plasma sheet boundary layer (PSBL) typically consist of unidirectional or counterstreaming ion beams strongly aligned to the magnetic field [e.g., *DeCoster and Frank*, 1979; *Forbes et al.*, 1981; *Lui et al.*, 1977, 1983; *Eastman et al.*, 1985; *Takahashi and Hones*, 1988; *Nakamura et al.*, 1992]. The importance of these ion beams for the transport of energy from the distant tail to the near-Earth region and their role in substorms have also been discussed [*Eastman et al.*, 1985; *Rostoker and Eastman*, 1987]. Quasi-steady reconnection at a site tailward of the observation point has been suggested as the source of these beams [e.g., *Schindler and Birn*, 1987; *Onsager et al.*, 1991].

0148-0227/02/2001JA007547

[3] High-speed flows have also been detected in the central plasma sheet (CPS) [e.g., *Hones*, 1979; *Nishida et al.*, 1981; *Cattell and Mozer*, 1984; *Huang et al.*, 1987; *Baumjohann et al.*, 1989, 1990; *Sergeev et al.*, 1992; *Angelopoulos et al.*, 1992, 1994; *Nagai et al.*, 1998; *Petrukovich et al.*, 2001]. These flows are highly time varying in nature and have properties radically different from the field-aligned beams observed in the PSBL. The CPS high-speed flows typically consist of a single bulk flow population having a significant convective component [*Nakamura et al.*, 1991; *Petrukovich et al.*, 2001], and are often accompanied by transient magnetic field dipolarization and ion heating [e.g., *Angelopoulos*, 1996; *Angelopoulos et al.*, 1992; *Nagai and Machida*, 1998; *Fairfield et al.*, 1999]. The relationship of these flows to substorms is central to the near-Earth neutral line model of substorms [e.g., *Hones*, 1979; *Baumjohann et al.*, 1991; *Nagai et al.*, 1998; *Nagai and Machida*, 1998; *Nakamura et al.*, 1999].

[4] The relative importance of the field-aligned PSBL beams and the CPS bulk flows for the transport of energy into the inner magnetosphere and their role in substorms are still under debate [*Lui et al.*, 2000]. The first step in assessing their relative importance is to investigate the frequency of occurrence of these fast flows, their spatial and temporal extents and their effects on the plasma sheet plasma properties and the magnetic field. With single-spacecraft observations, this information can only be obtained from statistical analysis of a large number of plasma sheet measurements.

[5] In statistical studies of high-speed flows in the plasma sheet involving a large amount of data, examining each and every particle distribution is often not feasible. Thus in most previous studies, moment-based selection criteria were used to distinguish between field-aligned beams and bulk flows. In *Baumjohann et al.*'s [1990] study using AMPTE/IRM data, it was assumed that field-aligned beams and bulk flows occur in the PSBL and CPS, respectively, and these two regions are distinguished from each other based on field strength, elevation angle, and photoelectron effects. In a study of bulk flows measured by AMPTE/IRM and ISEE 2, *Angelopoulos et al.* [1994] used the condition of plasma $\beta > 0.5$ and flow speed greater than 400 km/s in an attempt to eliminate PSBL samples from the CPS fast flow samples. Based on these selection criteria, *Angelopoulos et al.* [1994] found that high-speed bulk flows in the CPS account for a large fraction of the earthward mass and energy transport into the inner magnetosphere with numbers that vary in the range of 40–100% (depending on the local time) in the region tailward of $x_{GSE} = -15$ R_E. On the other hand, *Paterson et al.* [1998], in a more recent survey of Geotail data, concluded that high-speed bulk flows are primarily field aligned and do not contribute substantially to convection nor to the transport of magnetic flux into the inner magnetosphere.

[6] In a separate study, instead of selecting events based on spatial regions in the plasma sheet, *Nagai and Machida* [1998] selected convective bulk flows by requiring the x component of the perpendicular flow speed, $|v_{\perp,x}|$, to be greater than 300 km/s. The Nagai and Machida selection criterion ensures that a significant component of the flow is perpendicular to the magnetic field. They found that the onset of both earthward and tailward convective flows were closely related to the onset of substorms. A puzzling finding of the Nagai and Machida study is a strong dawn–dusk asymmetry in the occurrence of both earthward and tailward high-speed convective flows, with the great majority of events located in the premidnight sector. Such asymmetry was also found in *Nakamura et al.*'s [1991] survey of AMPTE/IRM high-speed flows in the vicinity of the neutral sheet but was attributed to orbital biases.

[7] In studies of bulk flows using moment-based selection criteria (without examining the actual particle distributions), the desired selection should maximize the inclusion of bulk flow events and minimize the contamination by field-aligned beam events. However, previously used selection criteria (e.g., $\beta > 0.5$ and flow speed > 400 km/s) may have included field-aligned beams, as recognized by *Angelopoulos et al.* [1994], though the severity of this problem has not been thoroughly investigated. Recently, *Chen et al.* [2000] questioned the true nature of high-speed bulk flows. They argued that bursty bulk flows observed in the CPS do not represent bulk motion of a single ion population, contrary to the conclusion reached by a large number of previous studies [e.g., *Baumjohann et al.*, 1989; *Nakamura et al.*, 1991; *Angelopoulos et al.*, 1992; *Nagai et al.*, 1998].

[8] In this study we survey all high-speed (>250 km/s) flow events observed by Wind in the near-Earth plasma sheet. With detailed examination of particle distributions observed in each high-speed flow event, we first demonstrate that the field-aligned beams and bulk flows observed in the near-Earth plasma sheet are distinct. By classifying high-speed flows based on their ion distribution characteristics rather than by spatial regions within the plasma sheet, we examine on an event by event basis the properties of the field-aligned beams and the bulk flows, in particular their spatial distribution and their associated thermal and magnetic variations. Using our classification we proceed to evaluate the performance of the previously used moment-based selection criteria for differentiating field-aligned beams from convective bulk flows. We also confirm the presence of a strong dawn–dusk asymmetry of the bulk flow occurrence rate found by *Nagai and Machida* [1998] and point out how moment-based selection criteria could affect this finding. The results of the present study should provide a basis for estimating the rate of plasma transport into the inner magnetosphere.

[9] Our survey is somewhat similar to the studies by *Nakamura et al.* [1991, 1992] of beams and bulk flows, respectively, in that the study is based on the examination of individual particle distribution. But unlike those studies, the present survey does not consider data from any one particular plasma sheet region. Thus the organization of the flow type by region is a consequence (rather than an assumption) of the study.

[10] The organization of this paper is as follows. In sections 2 and 3 the instrumentation and data selection are briefly described. Two individual events are presented in section 4 to illustrate the ion distributions in high-speed bulk flows and field-aligned beams. A statistical survey of the spatial distributions of these flows and their associated plasma and magnetic variations are described in section 5. In section 6 we discuss the implications of our observations for the origin of these flows. There we also evaluate moment-based selection criteria to differentiate bulk flows

from field-aligned beams. We summarize the findings in section 7.

2. Instrumentation

[11] This study uses data taken from the Wind spacecraft. Plasma parameters are obtained from the Three-dimensional Plasma and Energetic Particle (3DP) experiment, with varying time resolutions. Full 3D proton distributions were produced every spacecraft spin period (3 s) from the PESA-H detector, operating in a mode to detect ions with energies from 80 eV to 30 keV; 3D distributions of electrons with energies from a few eV to 30 keV were produced by the EESA-L and EESA-H detectors [*Lin et al.*, 1995]. Due to limited telemetry capacity, usually the 3 second distributions are averaged over 24 s before being transmitted; however, sometimes high time resolution burst mode data is available which lasts 6 min, during which the spacecraft transmits full-resolution (3 s) 3D ion and electron distributions. The burst mode is triggered by sudden enhancements of energetic (hundreds of keV) electron fluxes (detected by the silicon semiconductor telescopes) and was successful in capturing a number of high-speed bulk flow events. The magnetic field is measured at a rate of 10.9 samples/s [*Lepping et al.*, 1995], but for our analysis, the magnetic field data are averaged over 3 s.

3. Data Selection

[12] We use data from 17 Wind plasma sheet passes between 1995 and 1997. Wind was near the GSE equatorial plane for all of these crossings (Figure 1). The total time Wind spent in the plasma sheet (excluding lobe periods) is 333 hours (or 28500 plasma measurements). We examine all high-speed (>250 km/s) flows during these plasma sheet intervals. While the selection process begins with the magnitude of the flow speed, the categorization of the flows in terms of bulk flows and field-aligned beams is done by examining each individual ion distribution. During 14 of the high-speed flow events (all of which are bulk flows rather than field-aligned beams), 3 s resolution burst data were available.

[13] The present data set contains no orbital nor seasonal biases in terms of the spacecraft coverage of the plasma sheet (see Figure 12).

4. Individual Events

[14] In this section, we present examples of particle distributions observed during high-speed flows. These examples serve as prototypes for the categorization of high-speed flow events into two distinct categories, namely bulk flows and field-aligned beams, based on the nature of their ion distributions. The consequences of this categorization are the subject of the rest of this study.

[15] Although particle distributions characterizing high-speed flows and field-aligned beams have been shown in numerous previous studies (see Introduction), we feel it is important to reexamine their properties here for the purpose of demonstrating our event classification criteria. The illustration of individual particle distributions is also important in light of the recent studies by *Parks et al.* [1998] and *Chen et al.* [2000] who question the true nature of high-speed flows detected in the plasma sheet.

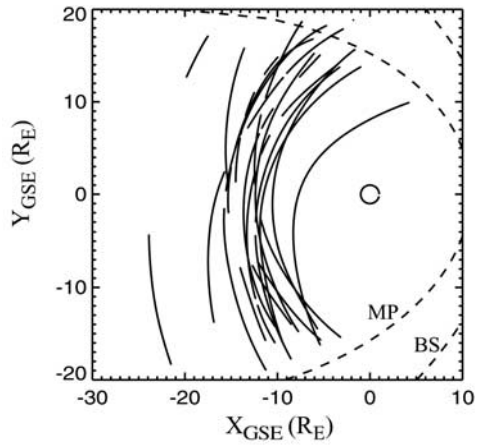

Figure 1. Coverage of the near-Earth plasma sheet by Wind in GSE $x-y$ plane in the period between September 1995 and October 1997. The discontinuous periods along the orbits indicate lobe encounters.

4.1. High-Speed Bulk Flow Events

[16] Figure 2 shows an example of a plasma sheet crossing by Wind. On 26 July 1997, Wind was in the premidnight region ($y_{GSM} \sim 7.5$ to 1.3 R_E) of the near-Earth plasma sheet ($x_{GSM} \sim -8$ to -11 R_E) at low latitude ($z_{GSM} \sim 0$ R_E) when it observed a series of high-speed plasma flows between 0400 and 0730 UT, reaching flow speeds greater than 400 km/s in several events (Figure 2c). The majority of these flows are earthward directed (Figure 2d). Associated with flow bursts are large fluctuations of the magnetic field (Figures 2i–2m) and sudden enhancements of energetic ion and electron fluxes (Figures 2n–2o). Figure 2m shows that some of the field fluctuations are accompanied by large magnetic field dipolarization (between 0540 and 0700 UT) while in other cases (between 0420 and 0540 UT) the magnetic field elevation angle generally changed by less than 20°.

[17] To examine the individual flow enhancements in more details, Figure 3 shows a zoom-in of one flow event in the 0626–0639 UT interval (between the 2 vertical dashed lines in Figure 2). This interval was chosen because high time resolution (3s full 3D ion and electron distributions) data were available.

[18] Figure 3c shows that the flow enhancement begins at approximately 0630 UT. The high-speed (>400 km/s) flow is sunward but is followed by an interval of ~200 km/s antisunward flows (Figure 3d). Coinciding with the flow enhancement, $|B_z|$ (Figure 3l) increases and $|B_x|$ (Figure 3j) decreases, resulting in an overall increase in the magnetic field inclination angle (Figure 3m). An increase of the ion temperature (Figure 3b) and decrease of the density (Figure 3a) also occurred during the high-speed flow. After the high-speed flow has subsided, the plasma parameters and the magnetic field gradually return to their original values before the flow enhancement encounter.

[19] Figure 4 shows two-dimensional cuts of the ion distributions at times labeled at the top of Figure 3. The

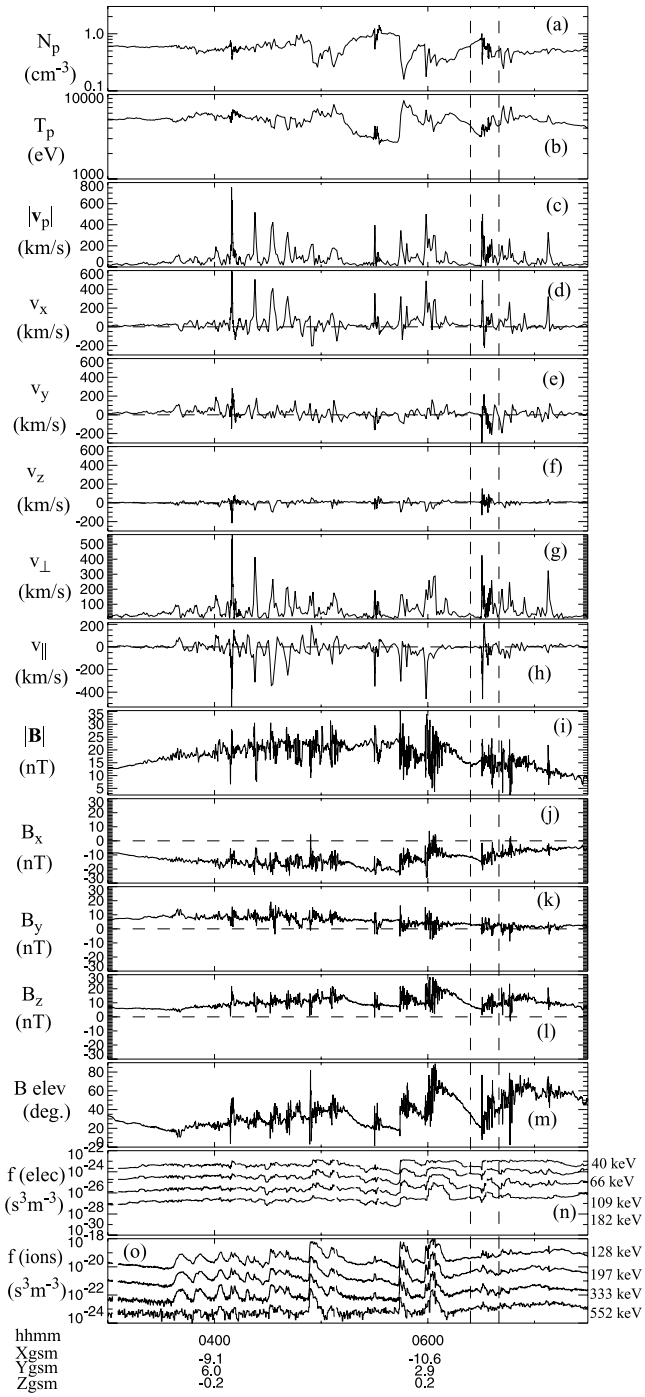

Figure 2. Wind encounters of a series of high-speed convective flows in the near-Earth plasma sheet on 26 July 1997. This figure shows the (a) total proton number density, (b) average proton temperature, (c) proton bulk speed, (d–f) GSM *x*, *y*, and *z* components of the flow velocity, (g–h) flow components perpendicular and parallel to the magnetic field, (i) magnetic field strength, (j–l) GSM *x*, *y*, and *z* components of the magnetic field, (m) magnetic field elevation angle defined by $\tan^{-1}[B_z/(B_x^2 + B_y^2)^{1/2}]$, (n) energetic electron phase space density, and (o) energetic ion phase space density. Most of the high-speed flows are accompanied by high-frequency magnetic field fluctuations and sudden increases of the field elevation angle and energetic particle phase space densities.

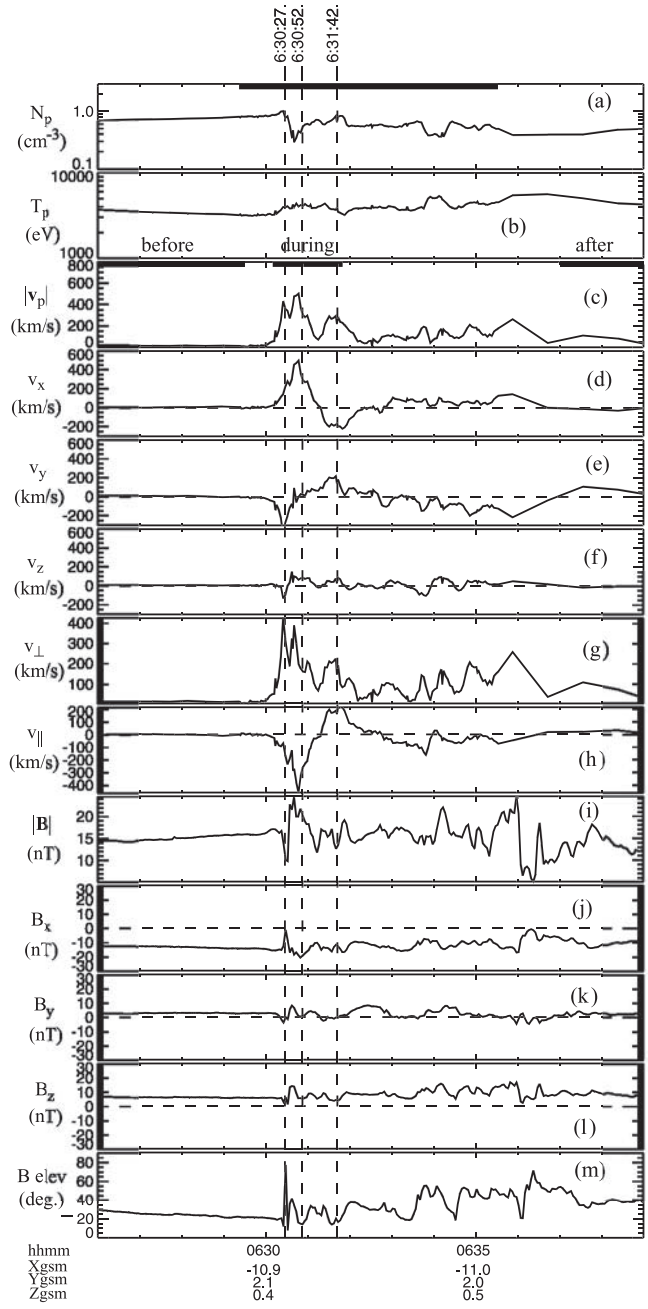

Figure 3. Zoom-in of Figure 2 showing a high-speed bulk convective flow event in detail. The parameters are similar to those of Figure 2. The horizontal bar in Panel a indicates the interval when high-resolution (3s) full 3D particle distributions are available. The three bars in Panel c indicate the intervals before, during, and after the high-speed flow detections.

sampling time for these distributions is 3 s. Figure 4a is a distribution taken at 063026 UT close to the neutral sheet ($B_x = -1.4$ nT). The distribution consists of a single population whose bulk velocity (indicated by the tip of the red line) is directed nearly along the sunward direction (indicated by the black line starting from the origin). The flow is directed $\sim 75°$ to the magnetic field. Figure 4b is a distribution taken 25 s later (at 063051 UT) when the spacecraft encountered a magnetic field B_x of -20 nT,

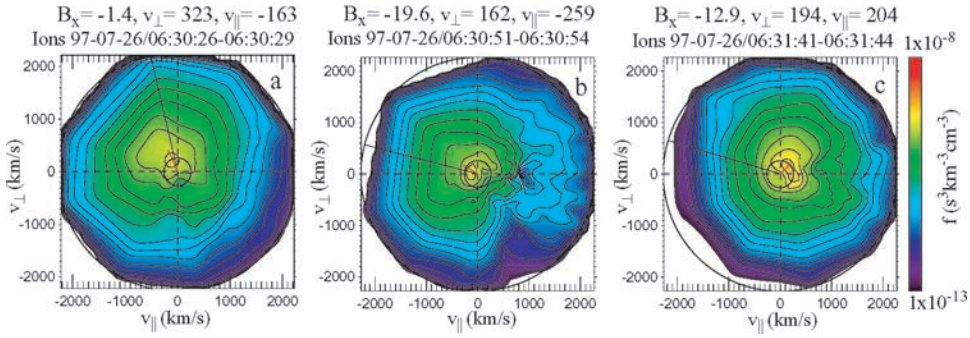

Figure 4. Two-dimensional cuts of 3D ion distributions, with 3-second sampling time. The *x* axis is aligned with the magnetic field. The *y* axis indicates the **E** × **B** (perpendicular to the magnetic field) direction. The black line indicates the sunward direction. The tip of the red line indicates the bulk velocity. The distributions are taken at times indicated at the top of Figure 3: (a) earthward flow near the neutral sheet, (b) earthward flow at higher latitude, and (c) tailward flow. All distributions consist of a single population. The ratio of perpendicular to parallel bulk speed is a function of the distance from the neutral sheet. The bulk flow is nearly perpendicular to **B** near the neutral sheet and nearly parallel at high magnetic latitude.

suggesting that the spacecraft is located at high magnetic latitude. The single-population bulk flow is again sunward (i.e., nearly along the black line), but more field aligned (~35° to the magnetic field), thus it has a smaller perpendicular component than in the previous example. Figure 4c shows a distribution obtained during the anti-sunward (and duskward) flow interval. The ion distribution again consists of a single population, convecting at 45° to the magnetic field.

[20] The particle distributions observed in other events throughout the 0400–0900 UT interval display similar characteristics as those just described in the above event. The distributions are all characterized by single-population bulk motion. The relative angle between the flow and the magnetic field depends simply on the magnetic field elevation angle. When detected at small $|B_x|$, i.e., near the neutral sheet, the flows are almost purely perpendicular to the magnetic field. It should be emphasized that because the field elevation angle remains high during many high-speed flow intervals (e.g., at 0600 UT), the ion distributions observed in these events display significant perpendicular components. Thus the convective nature of the flow is not merely an artifact of averaging a rapidly fluctuating magnetic field. At higher magnetic latitudes (larger $|B_x|$), the bulk flows are more field aligned. However, these field-aligned bulk flows are drastically different in character from field-aligned beams discussed in the next section.

[21] The particle and field behaviors just described are identical to those of high-speed bulk flows reported in previous studies [e.g., *Nakamura et al.*, 1991; *Angelopoulos et al.*, 1992; *Nagai et al.*, 1998]. It should be pointed out that the Wind spacecraft occasionally detected bulk flow events where a second, colder distribution is present during other plasma sheet passes [see also *Chen et al.*, 2000]. This cold population generally has the same **E** × **B** drift as the dominant distribution but its parallel velocity is usually much smaller. The cold ion population has previously been reported and interpreted as ionospheric [*Frank et al.*, 1996] or mantle [*Nagai et al.*, 1998] ions. For this type of two-population distributions, their velocity moments are generally dominated by the motion of the hotter population.

4.2. Field-Aligned Beam Events

[22] Figure 5 shows a plasma sheet crossing on 21 October 1997. Wind crossed the dusk flank magnetopause and entered the plasma sheet at ~2200 UT on 20 October. There were few occurrences of high-speed flows before 0640 UT on 21 October. A series of high-speed flows (Figure 5c) reaching flow speeds of 900 km/s were encountered at $X_{GSM} = -13$ to -14 R_E, $Y_{GSM} = 7$ to 5 R_E, $Z_{GSM} = -4$ R_E, just before the spacecraft entered the low-density lobe region at 0900 UT (Figure 5a). These flows were detected at large $|B_x|$ (Figure 5j), they were directed sunward (Figure 5d), were nearly purely field aligned (Figures 5g–5h), and were not accompanied by large fluctuations in the magnetic field (Figures 5i–5m) nor enhancements of the energetic particle fluxes (Figures 5n–5o).

[23] A zoom-in of a high-speed flow interval is shown in Figure 6. Four intervals of high-speed flows with flow speed exceeding 700 km/s occurred starting at ~0818 UT. These flows are dominated by $v_{||}$ (Figure 6h) and are earthward directed (Figure 6d). In addition, the magnetic field inclination angle (Figure 6m) is small (<10°) before, during and after the high-speed flow encounters. The plasma temperature (Figure 6b) during the high-speed flow interval is not significantly different from the periods preceding or following the fast flows. It is also noted that the high-speed flow intervals coincides with times of larger $|B_x|$ and $|\mathbf{B}|$ (Figures 6j and 6i), indicating that these flows are detected at high latitudes.

[24] Figure 7 shows 4 ion distributions at times labeled at the top of Figure 6, ordered by decreasing $|B_x|$, not by time. The distributions consist mainly of an earthward and tailward directed crescent-shaped beams. The earthward beam has large density while the tailward beam has higher energy. The beams detected at lower $|B_x|$ (Panels b and c) have lower low-energy cutoffs than those detected at higher $|B_x|$ (Panel a). The distributions in Panels b and c occurred at similar B_x and their characteristics are remarkably similar. This is

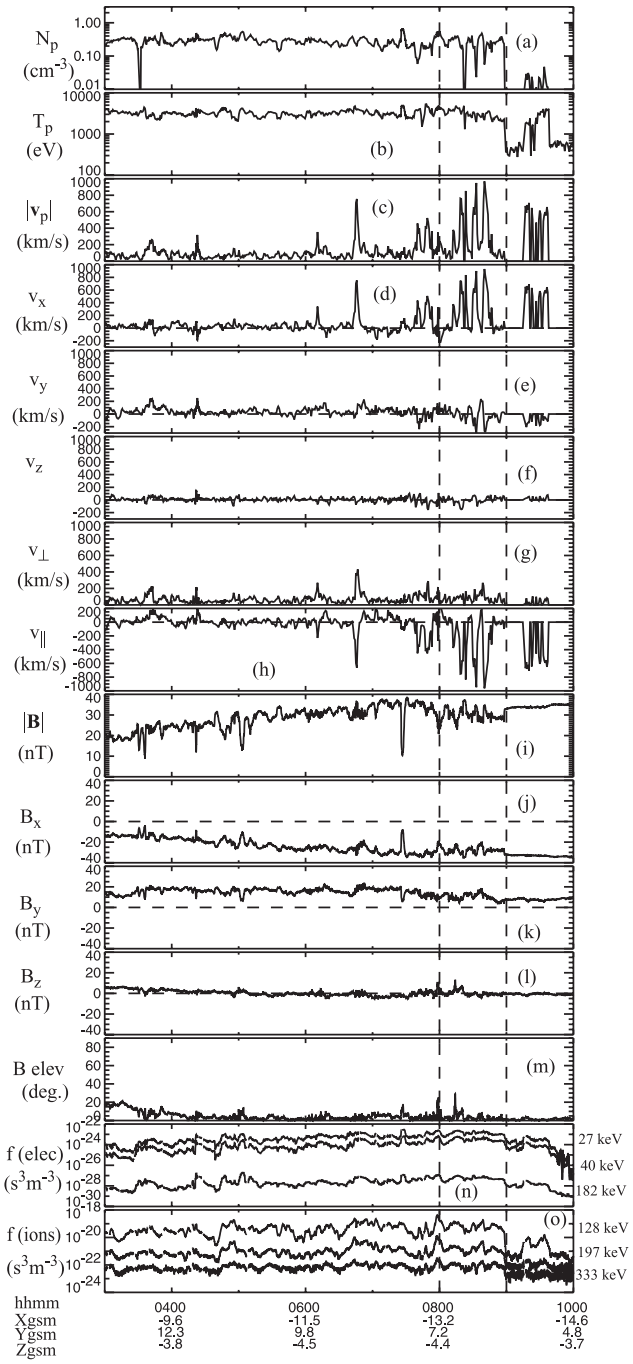

Figure 5. Wind encounters of a series of high-speed anti-field-aligned flows in the near-Earth plasma sheet (near the lobe) on 21 October 1997. The parameters are the same those shown in Figure 2. Unlike the convective flow cases in Figure 2, these field-aligned flows are not accompanied by high-frequency magnetic field fluctuations nor enhancements of the energetic particle fluxes. The magnetic field elevation angle remains low (<10°) throughout the high-speed flow intervals.

despite of the fact that distribution (c) was sampled 11 min after distribution (b), i.e., after the spacecraft had moved back and forth between different magnetic latitudes. At B_x = −22.7 nT (Panel d) the distribution is more isotropic. The two field-aligned beams are much closer to the origin than in the previous two cases. Besides the two beams, a third population seems to be present that is colder, has little parallel bulk speed while moving at the same perpendicular speed as the beam populations. This type of cold population is not common in other field-aligned beam events.

[25] Examination of other high-speed flows in the 0630–0840 UT interval shows that most of the beam characteristics just described are typical. The progression from a single unidirectional beam to two counterstreaming beams with low-energy cutoff, to two counterstreaming beams with a lower low-energy cutoff, to eventually a more stagnant isotropic distribution seems to be repeatable and

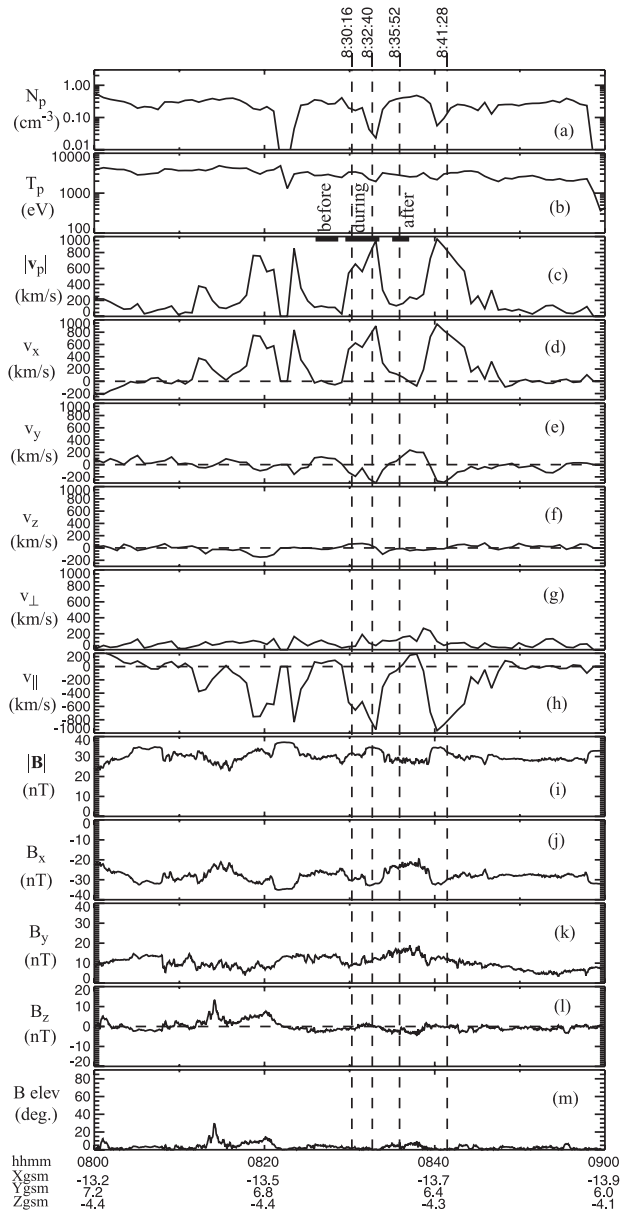

Figure 6. Zoom-in of Figure 5 showing high-speed flows in details. The high-speed flow intervals coincide with times of enhanced magnetic field strength. The three bars in Panel c (from left to right) indicate the periods before, during, and after the high-speed flow event centered at ~0831 UT.

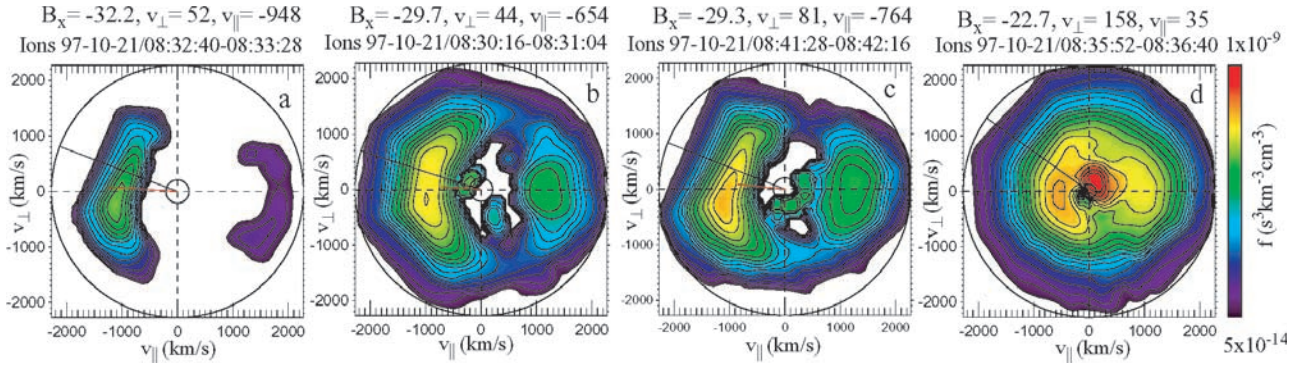

Figure 7. Two-dimensional cuts of 3D ion distributions, with 48-second sampling time. The distributions are taken at times indicated at the top of Figure 6, ordered by decreasing $|B_x|$ (i.e., decreasing distance from the neutral sheet). Distribution (c) was sampled 11 minutes after distribution (b), i.e., after the spacecraft had moved back and forth between different magnetic latitudes.

well organized with decreasing $|B_x|$, not by time. This behavior of the field-aligned beams indicates that the variation of the beam distributions is spatial rather than temporal. The existence of this stable plasma sheet structure has also been reported in previous studies [e.g., *Forbes et al.*, 1981; *Eastman et al.*, 1985; *Takahashi and Hones*, 1988; *Nakamura et al.*, 1991].

[26] It should be pointed out that field-aligned beams are easily distinguishable from bulk flows. Beams are crescent shaped, i.e., have low-energy cutoffs, whereas bulk flows are generally single drifting distributions, irrespective of whether their motions are parallel or perpendicular to the magnetic field. It is on the basis of this dramatic difference in the character of the particle distributions that we will classify high-speed flows in the Wind data set. The numerous differences between bulk flows and field-aligned beams in terms of their plasma and magnetic field properties, as well as their spatial occurrences, revealed in the next section provide further evidence that bulk flows and field-aligned beams are distinct phenomena.

5. Statistics

[27] To further investigate the properties of high-speed flows, we survey all high-speed ($|\mathbf{v}| > 250$ km/s) flows that occurred during the 17 Wind perigee passes (Figure 1). For each high-speed flow sample, we examine its ion distribution. The majority (if not all) of the ion distributions in high-speed flows fall into the two categories described in the previous section: (1) bulk motion of predominantly a single population, exemplified by the event in section 4.1 and previously discussed by, e.g., *Nakamura et al.* [1991] and *Angelopoulos et al.* [1992], or (2) unidirectional or counterstreaming field-aligned beams with low-energy cutoffs, exemplified by the event in section 4.2 and previously studied by, e.g., *DeCoster and Frank* [1979], *Forbes et al.* [1981], *Eastman et al.* [1985], *Takahashi and Hones* [1988], and *Nakamura et al.* [1992].

[28] Our analysis is significantly different from previous statistical studies in that we classify bulk flow and field-aligned beam events based on visual inspection of each ion distribution, not by criteria based on plasma moments or by regions where these flows are detected.

[29] *Data selection*. In order to investigate the consequences of high-speed flows on the plasma sheet properties, we need to compare plasma sheet observations before, during and after the detection of fast flows. For such a survey we therefore exclude events which took place immediately before or after an interval where the spacecraft was in the lobes. This selection criterion excludes a large number of field-aligned beam events which are often detected at the plasma sheet/lobe interface when Wind crossed this region on its way to and from the lobe. However, this exclusion of beam events does not affect our study because the occurrence rate of beam events is not the subject of our investigation. The above criteria yield 51 bulk flow events and 34 beam events. Each event includes the rise and fall of the flow speed and contains multiple samples of flow with speed exceeding 250 km/s. The total number of high-speed ($|\mathbf{v}| > 250$ km/s) plasma measurements within the 51 bulk flow events is 194 and within the 34 beam events is 203. Using these events, we proceed to examine the plasma and magnetic field variations around the events on an event by event basis, as well as spatial distributions of these flows. All events occurred in the region of $x_{GSM} = -24$ to -7 R_E, $y_{GSM} = -12$ to 15 R_E, and $z_{GSM} = -6$ to 6 R_E.

5.1. Spatial Distributions

[30] In this section we investigate the occurrence of bulk flows and field-aligned beams in terms of their location relative to the neutral sheet and in the ecliptic plane. As proxy for distance from the neutral sheet, we use three parameters: the x component of the magnetic field, the plasma β value, and the theoretical distance from the neutral sheet [*Fairfield*, 1980].

5.1.1. B_x

[31] Figure 8 shows the occurrence of high-speed ($|\mathbf{v}| > 250$ km/s) bulk flows and field-aligned beam measurements (within the 51 bulk flow and 34 beam cases) as a function of B_x. The top panels show unnormalized occurrence distributions. The bottom panels show occurrence distributions normalized by the total number of measurements in the plasma sheet irrespective of the flow speed. The bulk flows (left panels) have the highest occurrence frequency near the neutral sheet ($B_x \sim 0$), but are still detected out to $|B_x| \sim 25$

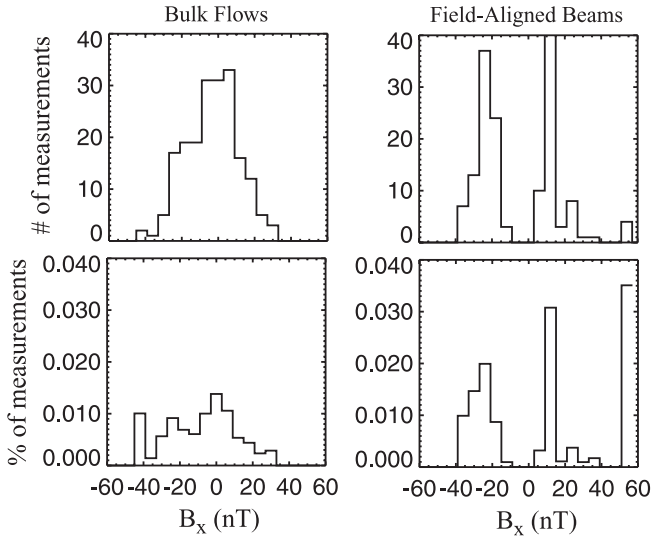

Figure 8. Distributions of high-speed ($|\mathbf{v}| > 250$ km/s) bulk flow (left panels) and field-aligned beam (right panels) plasma measurements as a function of the x component of the magnetic field. The top panels are unnormalized occurrence distributions. The bottom panels are normalized by the number of measurements in the plasma sheet irrespective of flow speed. The occurrence of bulk flows (field-aligned beams) is maximum (minimum) at the neutral sheet ($B_x = 0$). An extended B_x region exists where both bulk flow and field-aligned beam events are detected.

nT, while the beam events (right panels) occur primarily away from the neutral sheet ($|B_x| > 0$). Some beam events were detected rather close to the neutral sheet (down to $|B_x| \sim 5$ nT), but none occurred in the neutral sheet ($B_x = 0$) itself. Thus the neutral sheet is the site where only bulk flows are detected, whereas at higher latitudes both beams and bulk flows can occur, with the probability of detecting beams (bulk flows) increasing (decreasing) with increasing distance from the neutral sheet. The extended overlapping region (say 5 nT < $|B_x|$ < 25 nT) where both bulk flows and beams are present makes it impossible to distinguish bulk flows from beams based solely on the value of B_x. It should be pointed out that the low occurrence rate of the beams at 20 nT < $|B_x|$ < 30 nT is due to our exclusion of events that immediately precede or follow lobe encounters. Furthermore, many counterstreaming beams have low "bulk speed" thus do not satisfy the high-speed flow criterion, $|\mathbf{v}| > 250$ km/s, even thought the individual beams have significant speeds. Thus, the overall low rate (<4%) of beam encounter should not be taken to indicate that field-aligned beams are uncommon in the PSBL.

5.1.2. Plasma β

[32] Another indication of the distance from the neutral sheet is the β value [e.g., *Angelopoulos et al.*, 1994]. β is highest in the neutral sheet and decreases with increasing distance from the neutral sheet. Figure 9 shows the normalized occurrence distribution of the bulk flow (left panel) and beam (right panel) measurements as a function of β. The probability of detecting bulk flows becomes significant at β > 0.5. The field-aligned beams, on the other hand, has a highest detection frequency below β = 2. It is noted that a significant number of beam cases were still detected between β = 0.5 and 1. The consequences of this finding in terms of the previously used moment-based selection criteria will be discussed in section 6.3.

5.1.3. Z_{ns}

[33] Figure 10 shows the normalized occurrence of bulk flows and beams as a function of the theoretical distance from the neutral sheet [*Fairfield*, 1980]. The distributions are somewhat similar to those of B_x. The bulk flow distribution has a slight peak at the theoretical neutral sheet ($Z_{ns} = 0$ R_E) where the beam distribution has a deep minimum.

5.1.4. Spatial Distribution in Ecliptic Plane

[34] The occurrence of high-speed bulk flow and field-aligned beam events in the GSM equatorial (x–y) plane is shown in Figure 11. The top panels show the velocity vectors at the location of space at which the event occurred. The velocity displayed is the maximum velocity achieved during the event. Essentially all bulk flows are earthward directed. Remarkably, 41 of the 51 bulk flow events occur on the dusk side ($y_{GSM} > 0$), 10 occurred on the dawn side. For the beam events, half (17 of 34 events) occurred at $y_{GSM} > 0$, the other half at $y_{GSM} < 0$.

[35] The bottom panels of Figure 11 show the perpendicular component of the velocity vectors taken at the time of maximum velocity achieved. Here, many of the bulk flow events continue to have relatively high perpendicular flow speeds, while as expected, virtually all the perpendicular flow speeds for the beam events are close to zero. This

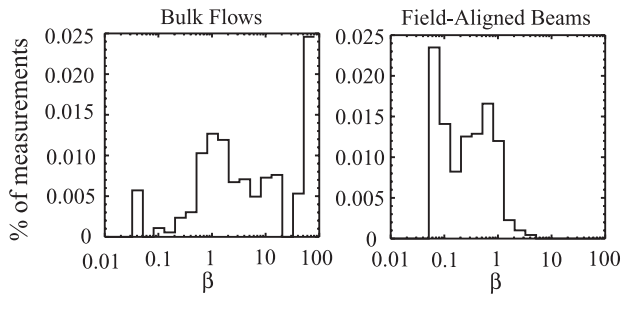

Figure 9. Normalized distributions of high-speed ($|\mathbf{v}| > 250$ km/s) bulk flow (left panels) and field-aligned beam (right panels) plasma measurements as a function of the plasma β.

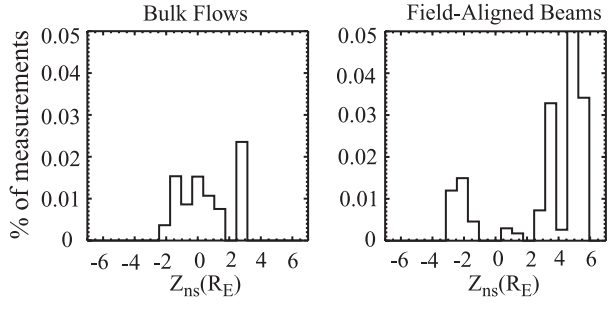

Figure 10. Normalized distributions of high-speed ($|\mathbf{v}| > 250$ km/s) bulk flow (left panels) and field-aligned beam (right panels) plasma measurements as a function of the theoretical distance from the neutral sheet. The distributions are similar to Figure 8.

shows that, although the bulk flow events were selected only based on their bulk flow character, not based on large perpendicular flow speed, the majority of our events have a significant convective flow component. It is also noted that essentially all bulk flows detected by Wind are earthward directed. These flows do not show significant duskward or dawnward drift on average.

5.1.5. Occurrence of Bulk Flows in B_x-Y_{GSM} and $Z_{ns}-Y_{GSM}$ Planes

[36] Figure 12 shows the occurrence of high-speed bulk flow measurements within the 51 high-speed bulk flow events in the B_x-y_{GSM} and $Z_{ns}-y_{GSM}$ planes, representing a view of the occurrence of these flows in a $y-z$ cross section of the plasma sheet. The top panels are the unnormalized distributions showing that the majority of the events occurred in the dusk sector ($y_{GSM} > 0$). The middle panels show the Wind coverage in these planes. The coverage is rather symmetric about midnight and about the neutral sheet ($B_x = 0$ and $Z_{ns} = 0$). Thus the normalized distributions (bottom panels) still show a preference for bulk flow to occur on the dusk side plasma sheet; i.e., orbital biases do not appear to be the cause for the dawn–dusk asymmetry. In section 6.4 we will investigate the dawn–dusk asymmetry in the occurrence of bulk flow events in more detail.

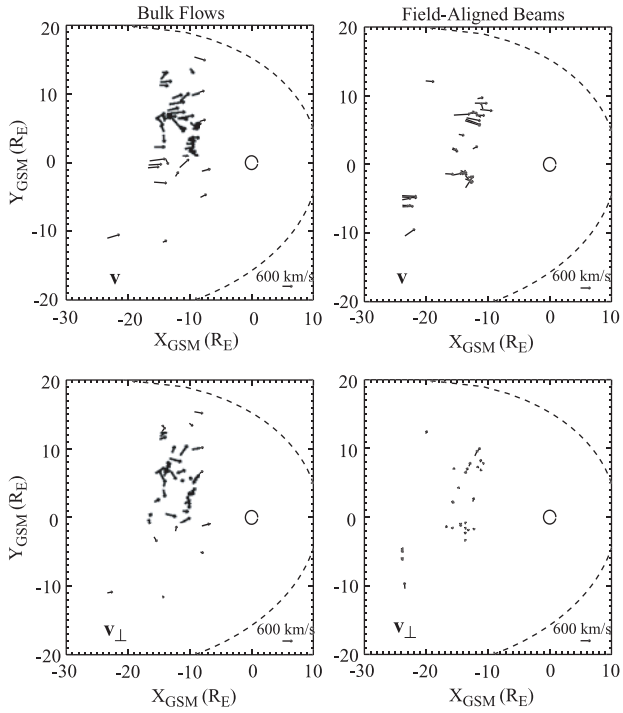

Figure 11. Occurrence of high-speed bulk flows (left panels) and field-aligned beams (right panels) in the GSM equatorial ($x-y$) plane. Top panels show the maximum flow velocity vectors achieved during the events. Bottom panels show the perpendicular component of the velocity taken at the time of maximum flow speed. Most high-speed bulk flow events occur on the dusk side. Field-aligned beams are more evenly distributed about midnight.

5.2. Magnetic Field Variations Associated With Bulk Flows and Field-Aligned Beams

[37] We now investigate the variations of the magnetic field associated with the occurrence of high-speed flows in the plasma sheet on an event by event basis (Figure 13). For each event, we compared the magnetic field elevation angle, $\tan^{-1}[B_z/(B_x^2 + B_y^2)^{1/2}]$, measured before the event with the field angle measured during the high-speed flow interval (top panels), as well as the angle after the event (middle panels). The bottom panels show the maximum field angle achieved during the high-speed flows. The times representative of "before," "during," and "after" intervals are denoted by horizontal bars in Figures 3c and 6c. The "before" and "after" intervals are times where the values of the magnetic field and electron temperature were relatively stable before the velocity began to rise and after the flow returned to its near-stagnant state, respectively. The "before," "during," and "after" values are the average values of the parameters in these intervals.

[38] For the field-aligned beam events (right panels), the average field elevation angle is rather low before, during, and after the high-speed flow interval and this angle does not change significantly from its value before the event to its value during and after the detection of the high-speed beams. These findings indicate that the beams tend to occur in regions of highly stretched and stable field lines.

[39] The bulk flow events (left panels), on the other hand, occur at a wide variety of magnetic field elevation angles. The average field angle achieved during high-speed bulk flows tends to be enhanced compared to before the event (most points lie above the diagonal line). This field angle enhancement is even more pronounced if one compares the maximum field angle achieved during the event to the maximum angle before the event (bottom panel), and for many events, the field angle remains enhanced even after the detection of the bulk flows (middle panel). Note that for cases when the elevation angle is already large before the bulk flow encounter, this field angle does not change during or after the detection of bulk flow. There are also a number of bulk flow cases where the field elevation angle is low before, and remains low during, and after the detection of fast flows. These are the cases that lie close to the diagonal line at low field angle (in top, middle, and bottom left panels) and imply that these bulk flows are not accompanied by field dipolarization. The variety of degree of field dipolarization within bulk flow events just discussed is also apparent in the series of individual events shown in Figure 2. Finally, there are essentially no data points below the diagonal line, indicating that the field angle during the bulk flows is almost never reduced from its value before the flow encounter.

5.3. Plasma Temperature Variations

[40] We now investigate the thermal properties of the plasma sheet in association with bulk flows and beams on an event by event basis. We shall use electron temperature instead of ion temperature because the ion temperature computed from the Wind 3DP measurements is lower than its true value at temperatures above 5 keV because of the 30 keV upper energy limit of the ion analyzer. However, the ion temperature behavior can be deduced from that of the

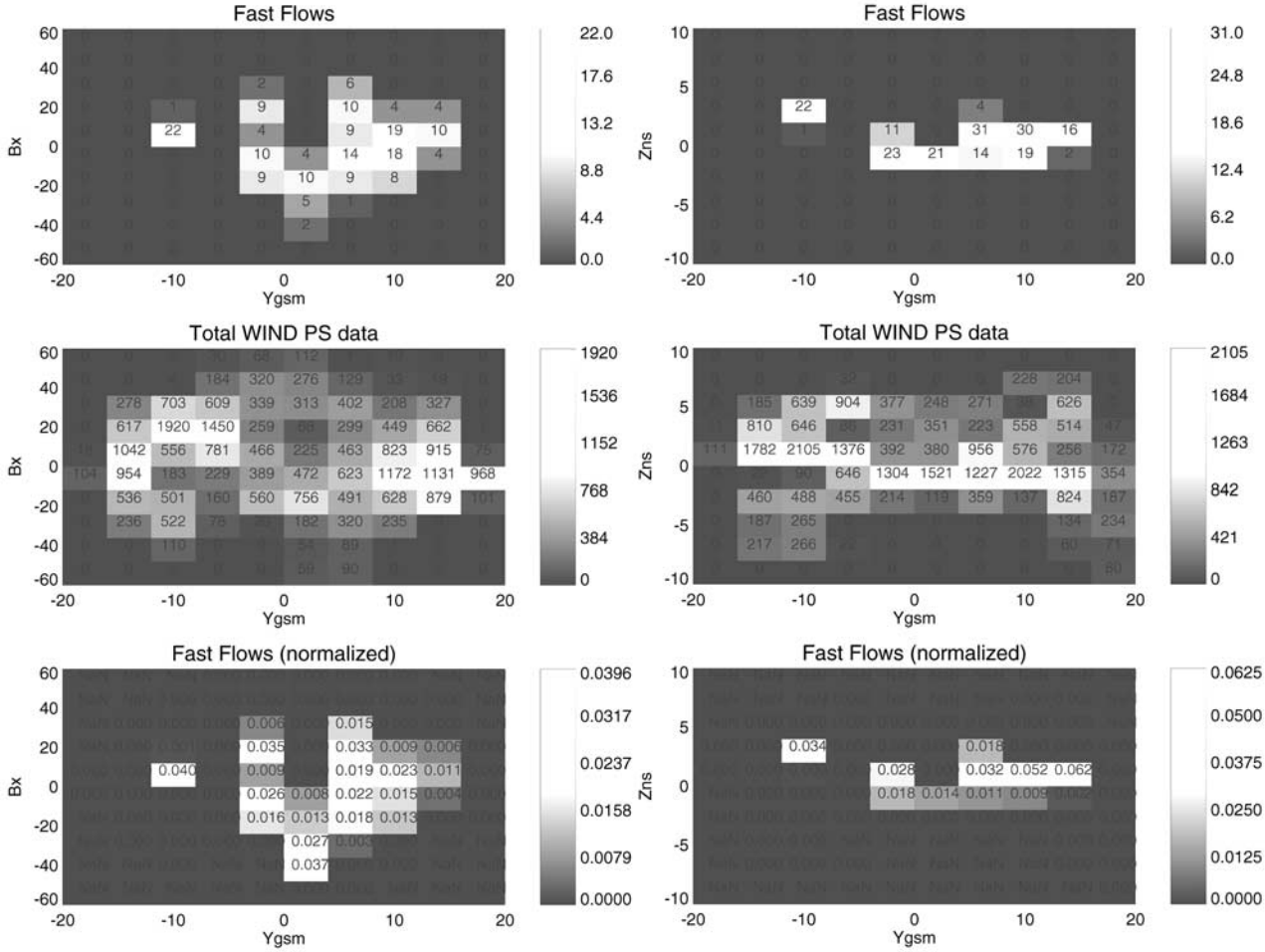

Figure 12. Occurrence of high-speed bulk flows in the B_x-y_{GSM} and $Z_{ns}-y_{GSM}$ planes, representing a view of the occurrence of these flows a $y-z$ cross section of the plasma sheet. The top panels are the unnormalized distributions. The middle panels show the Wind coverage in these planes. The normalized distributions (bottom panels) show a preference for bulk flow to occur on the dusk side plasma sheet.

electrons because the ratio of ion to electron temperature is approximately 6 throughout the near-Earth plasma sheet [*Baumjohann et al.*, 1989].

[41] Figure 14 shows a comparison between the electron temperature before, during, and after the event. The beam events (right panels) showed no clear increase in electron temperature during or after the event from its value before the flow encounter as most data points lie along the diagonal line, whereas the bulk events (left panels) are often (but not always) accompanied by an enhancement in the electron temperature. For bulk flow cases where the electron temperature is low before the detection of fast flow, the temperature increase during the bulk flows is substantial (the data points are far above the diagonal line), but for cases where the initial temperature is already high, the temperature is not further enhanced during the bulk flows. The temperature increase associated with bulk flows persists even after the flow has subsided: The data points continue to lie far above the diagonal line in the bottom left panel.

[42] To further investigate the temperature variations associated with bulk flows, Figure 15a shows the dependence of the temperature enhancement on the B_x value (a proxy of the location of the spacecraft relative to the neutral sheet) before the arrival of the high-speed bulk flows. It is seen that the electron temperature detected by the spacecraft is not enhanced if the spacecraft resides initially near the neutral sheet ($B_x = 0$). The temperature enhancement is large if the spacecraft is initially located at large $|B_x|$ (i.e., further from the neutral sheet). Based in part on this finding, we discuss in section 6.2 the possibility that the temperature increase could be a spatial effect rather than true heating of the plasma sheet plasma.

6. Discussion

[43] In this section we first discuss the relationship between bulk flows and field-aligned beams, followed by a discussion of the source of the temperature enhancement associated with bulk flows. We search for the optimal moment-based selection criteria for the identification of bulk flows and discuss how selection criteria can affect the results of statistical surveys of the occurrence and properties of bulk flows. Using the new selection criteria, we then perform an expanded statistical survey of bulk flows in the Wind data set, focusing especially on the

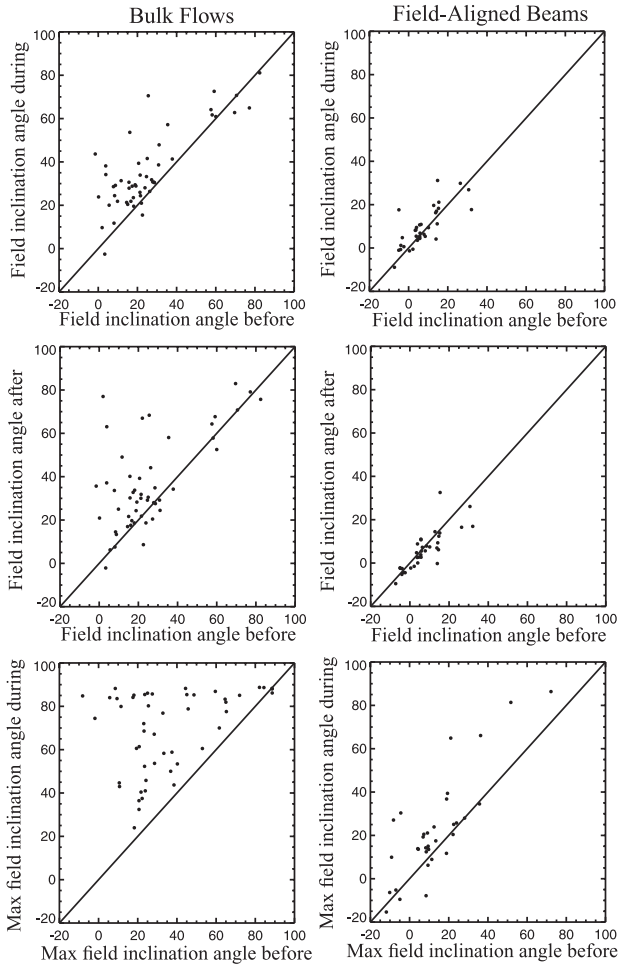

Figure 13. Changes of the field inclination angle associated with bulk flows (left panels) and field-aligned beams (right panels). Top panels show the average field elevation angle "during" the high-speed flows versus the average field angle in a period preceding the flow enhancements. Middle panels show the average field elevation angle in a time interval immediately after the encounter of high-speed flows versus the average field angle before the flow enhancements. Bottom panels show the maximum field elevation angle achieved during the encounter of high-speed flows versus the maximum field angle achieved in a period before the flow enhancements. The representative "before," "during," and "after" intervals are shown by horizontal bars in Figures 3c and 6c. Field-aligned beams are not accompanied by changes in field inclination angle, whereas bulk flows are often (but not always) accompanied by field dipolarization.

possible dawn–dusk asymmetry in the occurrence of these flows.

6.1. Field-Aligned Beams and Bulk Flows

[44] In this section we will discuss the differences between field-aligned beams and bulk flows based on the results from the individual event studies (sections 4.1 and 4.2) and the statistical analyses presented in section 5. Although bulk flows and field-aligned beams are similar in terms of their velocity moments and they may occur at the same magnetic latitudes, the dramatic differences between their properties highly suggest that they are distinct phenomena.

6.1.1. Field-Aligned Beams

[45] The field-aligned beams detected by Wind are identical to those reported in previous studies [e.g., *DeCoster and Frank*, 1979; *Forbes et al.*, 1981; *Eastman et al.*, 1985; *Nakamura et al.*, 1992]. The beams generally have crescent shapes (see Figure 7), having low-energy cutoffs. The beam distributions are organized by magnetic latitude rather than by time series. At large $|B_x|$ (presumably high magnetic latitude) regions one often detects only single earthward direct beams. As the spacecraft moves to smaller $|B_x|$ (lower latitude) regions, counterstreaming beams are observed with the earthward beam having higher density and lower low-energy cutoff than the tailward directed beam. At even smaller $|B_x|$ regions (i.e., closer to the neutral sheet) the low-energy cutoff of the two beams are lower, until the two beams merge to become a single and stagnant hot population. This progression of the beam evolution has previously been shown by *Forbes et al.* [1981], *Takahashi and Hones* [1988], and *Nakamura et al.* [1992] and interpreted as signatures of distant-tail reconnection [*Onsager et al.*, 1991], although this interpretation has never been confirmed due to the lack of simultaneous measurements of distant-tail reconnection.

[46] For counterstreaming beams the velocity moments calculated are not representative of bulk motions of the plasma. Beams having a velocity moment of $|\mathbf{v}| > 250$ km/s

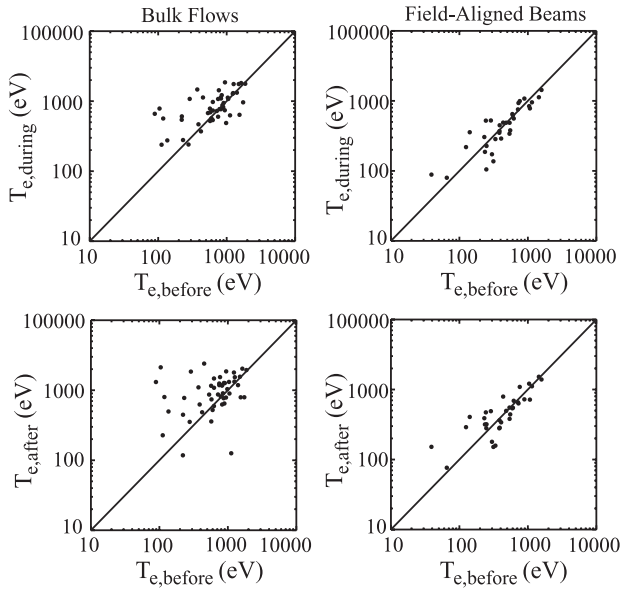

Figure 14. Changes of the electron temperature associated with the detections of bulk flows (left panels) and field-aligned beams (right panels). Top panels show the average temperature during versus before the high-speed flows detection. Bottom panels show the average field elevation angle immediately after versus before the encounter of high-speed flows. Field-aligned beams are not accompanied by changes in the temperature, whereas bulk flows are often (but not always) accompanied by temperature enhancements.

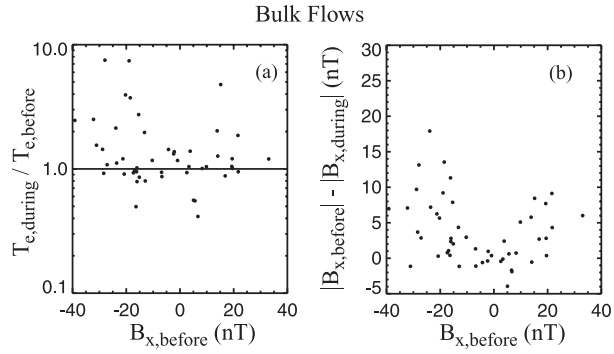

Figure 15. (a) Changes of the electron temperature from before to after the high-speed flow encounters as a function of the *x* component of the magnetic field measured before the high-speed bulk flow detection. (b) Changes of B_x from before to after the high-speed flow encounters as a function of B_x measured before the bulk flow detection.

are seen primarily at high latitudes, although some beam events have been detected rather close to the neutral sheet (down to $|B_x| \sim 5$ nT), but none occurred in the neutral sheet ($B_x = 0$) itself (Figure 8, right panels). The detections of beam events not far from the neutral sheet have also been reported by *Nakamura et al.* [1991] and *Nagai et al.* [1998].

6.1.2. Bulk Flows

[47] High-speed bulk flows, on the other hand, represent bulk motion of a predominantly single population, with no low-energy cutoff. They are detected in the neutral sheet as well as at higher latitudes, with peak occurrences at the neutral sheet. Bulk flows are directed mostly sunward, independent of the local magnetic field direction. Whether the flow has a large convective component or not depends on the location of observation relative to the neutral sheet, or on the state of magnetic field dipolarization. In the neutral sheet ($B_x = 0$), the flow is almost purely perpendicular to the magnetic field. At higher magnetic latitudes the flow becomes more and more field aligned. However, the ion distributions of field-aligned bulk flows are drastically different from field-aligned beams: They are well represented by a single drifting population and do not have low-energy cutoffs as seen in beams.

6.1.3. Bulk Flows are Not the Low-Latitude Counterparts of Field-Aligned Beams

[48] To investigate possible connections between bulk flows and beams, we have examined all beam events in our data set in search of evidence for spatial evolution from a single earthward beam to two counterstreaming beams, and to high-speed bulk flows as the spacecraft traverses the plasma sheet from the lobe toward the neutral sheet. Such a finding would indicate that beams and bulk flows are the same phenomenon just viewed at different latitudes in the plasma sheet. We have not found such an example. Instead, the high-latitude beams always evolve into an isotropic and stagnant population (instead of high-speed bulk flows) at lower magnetic latitudes [see also *Eastman et al.*, 1985]. The additional differences between the beams and bulk flows in terms of presence/absence of magnetic field dipolarization (Figure 13), temperature increase (Figure 14), energetic particle flux enhancements (Figures 2 and 5), and spatial distribution (Figures 11 and 12) for the 2 types of flows provide further evidence that bursty bulk flows and beams are indeed distinct and suggest that they are generated either at different locations in the tail or by different mechanisms.

6.2. Nature of Temperature Enhancements Associated With Bulk Flows

[49] In the analysis of the electron temperature variations associated with bulk flow events (section 5.3), we found that the plasma temperature increases, on average, in association with the detection of bursty bulk flows, in agreement with the results of the superposed epoch analysis by *Angelopoulos* [1996]. Closer inspection of the individual events, however, indicates a variety of temperature behavior, with some cases showing no temperature enhancements at all. Typically, no temperature enhancements are observed if the spacecraft is located at small $|B_x|$ (i.e., near the neutral sheet) before the detection of bursty bulk flows, whereas for cases where the spacecraft is initially located at larger $|B_x|$ (presumably further away from the neutral sheet) a significant increase in the temperature is detected (Figure 15a). Figure 15b shows that events where the spacecraft is initially in the small $|B_x|$ region remains in that region during the high-speed flows whereas the spacecraft that initially resides at large $|B_x|$ tends to end up at lower $|B_x|$ at the time when the high-speed flow is detected. The findings in Figures 15a and 15b raise the question of whether the temperature increase is indicative of true heating of the plasma sheet plasma or if it is merely a spatial effect due to the thickening of the plasma sheet associated with the arrival of the high-speed flows causing the spacecraft that is initially at high magnetic latitude to effectively move to lower magnetic latitude where the plasma sheet is hotter. A spacecraft that is situated initially near the neutral sheet does not move relative to the neutral sheet when the plasma sheet thickens and would not detect any temperature change.

6.3. Evaluation of Moment-Based Selection Criteria for Bursty Bulk Flows

[50] In this section, we first compare our categorization of the beam and bulk flow events based on the characteristics of the ion distributions with moment-based selection criteria used in previous statistical investigations by *Angelopoulos et al.* [1994] and *Nagai and Machida* [1998]. We then search for the optimal moment-based selection criteria. Such moment-based criteria are useful when surveying a large data set where inspecting each particle distribution is not feasible.

6.3.1. Plasma β

[51] In Figure 9, it was shown that a large number of field-aligned beam events with flow speed >250 km/s were also detected in regions with $\beta > 0.5$, the effect of which we now discuss. The top panel of Figure 16a shows the percentage of bulk flow plasma measurements with flow speed >250 km/s (within the 51 bulk flow events of section 5, each event containing multiple samples of flow with speed exceeding 250 km/s) that would be omitted as a function of the β threshold value, while the bottom panel shows the percentage of field-aligned beam measurements with flow speed >250 km/s (within the 34 beam events) that would satisfy the

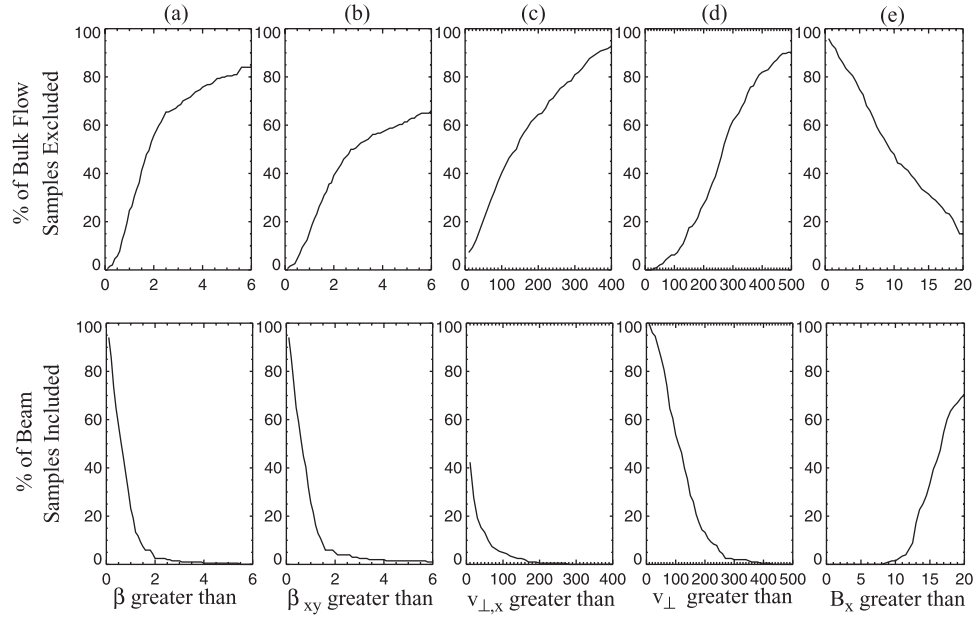

Figure 16. Top panels show the percentage of high-speed (>250 km/s) bulk flow plasma measurements excluded by the selection criterion. Bottom panels show the percentage of high-speed (>250 km/s) field-aligned beam measurements that satisfies the selection criterion. The $\beta_{xy} > 2$ and $v_{\perp} > 250$ km/s regimes contain less than 5% of the field-aligned beam samples while retaining ~60% of bulk flow samples.

β condition. If one includes all events with $\beta > 0.5$, more than 95% of the bulk flow measurements would be included (i.e., few omitted) which is desirable. However, a large number (~55%) of undesired field-aligned beam samples would also satisfy this condition (bottom panel of Figure 16a). If on the other hand, one were to impose a higher β threshold value, say $\beta > 2$, only 5% of the beam measurements satisfy this condition, and at the same time ~55% of the bulk flow samples would be omitted with this stricter criterion. To increase the β threshold value further does not reduce the number of beam events significantly while excluding more bulk flow events. The exclusion of bulk flow events at higher β is due partly to the fact that bulk flows tend to occur in conjunction with field dipolarization, resulting in an increase of B_z and a decrease of β. Thus increasing the β value does not necessarily correspond to restricting the survey region closer to the neutral sheet. To avoid this problem, the better β parameter should include only B_x and B_y in the magnetic pressure term (see below).

[52] We have performed the same analysis but by imposing the $v_p > 400$ km/s condition (as in *Angelopoulos et al.*'s [1994] study) instead. The results are not significantly different from the $v_p > 250$ km/s case. The percentage of field-aligned beams that satisfy the $\beta > 0.5$ condition is reduced slightly to ~50% (from 55% for the $v_p > 250$ km/s case).

6.3.2. Plasma β Based on B_x and B_y (β_{xy})

[53] As discussed above, β_{xy} is a better indicator of the distance from the neutral sheet than β. Figure 16b shows the results if one imposes a selection criterion based on β_{xy}. The percentage of bulk flow samples excluded by the β_{xy} condition is much lower than for the β condition, especially at high β, while the percentage of beam samples included is nearly the same for the two conditions. If one imposes the $\beta_{xy} > 2$ condition, less than 5% of beam samples are included while ~60% of bulk flow samples are retained, a significant improvement over the $\beta > 2$ condition.

6.3.3. $V_{\perp,x}$

[54] Figure 16c shows the results if one imposes a condition on the minimum value of $v_{\perp,x}$. For the condition of $v_{\perp,x} > 300$ km/s used by *Nagai and Machida* [1998], none of the beam samples would be mistakenly included (bottom panel). At the same time, only 20% of the bulk flow samples would satisfy this strict selection criterion (top panel). If one relaxes the threshold to $v_{\perp,x} > 200$ km/s, one would miss ~65% of the bulk flow samples while less than 1% of the beam samples would be included.

6.3.4. $v_{\perp}$

[55] If one imposes a more general condition on the convective flow speed, $v_{\perp}$, instead of the directional $v_{\perp,x}$, Figure 16d is obtained. A $v_{\perp} > 250$ km/s condition would ensure that only ~5% of the beam events satisfy this condition (bottom panel) while only 45% of the bulk flow events are omitted (top panel).

6.3.5. B_x

[56] In the near-Earth plasma sheet, one of the better indicators of the distance from the neutral sheet is the x component of the magnetic field. As has been shown in Figure 8, the bulk flow occurrence rate increases with decreasing $|B_x|$, i.e., decreasing distance to the neutral sheet, while the beam occurrence rate is opposite. Figure 16e shows that with a selection criterion of $|B_x| < 5$ nT, none of the beam cases would be included (bottom panel) while 80% of the bulk flow events are omitted (top panel). If one increases the threshold to 10 nT, ~2% of beam and 45% of bulk flow events satisfy this condition.

6.3.6. Summary

[57] It is evident from the results in Figure 16 that any of the parameters—β, β_{xy}, $v_{\perp,x}$, $v_\perp$, or B_x—can serve to select the desired beam or bulk flow populations. However, for none of the parameters is there a single threshold value that can clearly separate the bulk flow from the beam samples; a range of values of these parameters always exists where both types of fast flow are detected. The choice of the optimal selection criterion depends on the application. In studies of bulk flows within a restricted region around the neutral sheet for example, the $\beta > 2$ criterion can be used with minimal mixing of beam events. However, this condition also omits a large fraction of bulk flow events since bulk flows tend to occur in conjunction with field dipolarization which result in low β. Thus if one's objective is to account for as many bulk flow events as possible with minimal beam contamination, $\beta_{xy} > 2$ and $v_\perp > 250$ km/s may be the optimal selection criteria. The $\beta_{xy} > 2$ condition is particularly suitable for studies of relative transport by high-speed bulk flows when the survey is to be restricted to a region close to the neutral sheet. Alternatively, one could impose a combination of criteria, e.g., $\beta_{xy} > 0.5$ and $v_\perp > 250$ km/s. The β_{xy} condition restricts the survey to a certain region in the plasma sheet while the $v_\perp$ condition ensures that most high-speed flows in the region are bulk flows.

[58] It should be emphasized that our evaluation of the moment-based selection criteria is based on plasma sheet samples in the near-Earth ($x_{GSE} > -20\ R_E$) region and may or may not be applicable to the more distant plasma sheet.

6.4. Wind Bulk Flow Statistics Based on New Moment-Based Selection Criteria

[59] Using the moment-based selection criteria described in section 6.3, we examine the occurrence of bulk flows in the near-Earth plasma sheet. We also reexamine the possible dawn–dusk asymmetry in the occurrence of high-speed bulk flows using a slightly bigger data set.

6.4.1. Occurrence of High-Speed Bulk Flows in the Vicinity of the Neutral Sheet

[60] By imposing the condition of $\beta_{xy} > 2$, we ensure that the region surveyed is close to the neutral sheet and the high-speed samples are of bulk flows with minimal field-aligned beam contamination. Figure 17 shows the percentage of measurements as a function of $v_{\perp,x}$. The occurrence rate of large $v_{\perp,x}$ samples which satisfy the $\beta_{xy} > 2$ condition is similar to the rate for $\beta > 0.5$ (shown by *Angelopoulos et al.* [1999]). This is because large perpendicular flows automatically imply bulk flows (rather than beams) irrespective of the imposed β condition even though the $\beta > 0.5$ condition alone may have included beam events. The occurrence rate of $v_{\perp,x} > 250$ km/s is $\sim$0.2%.

6.4.2. Dawn–Dusk Asymmetry

[61] In Figures 11 and 12 we showed that the occurrence of high-speed bulk flow events has a dawn–dusk asymmetry, with higher occurrence in the premidnight region of the plasma sheet, while beam events seem to occur with equal probability on both sides of midnight. This finding is consistent with the Geotail results reported by *Nagai and Machida* [1998]. A similar dawn–dusk asymmetry was reported by *Nakamura et al.* [1991] based on the analysis of AMPTE/IRM data. However, in that study Nakamura et al. attributed the asymmetry to spacecraft orbital biases. Here we investigate the question of dawn–dusk asymmetry in more depth with a slightly larger data set than the one shown in Figures 11 and 12. Our analysis indicates that data selection criteria can strongly affect the finding on the presence/absence of a dawn– dusk asymmetry.

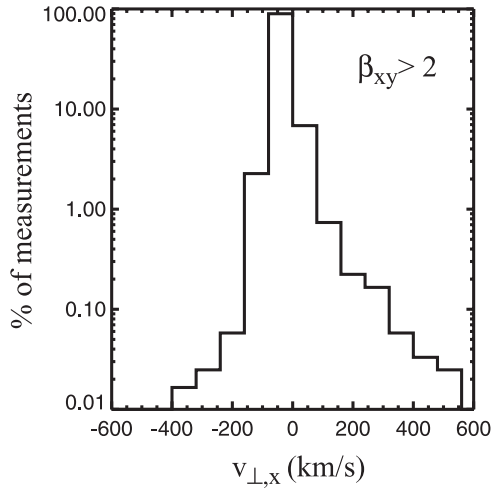

Figure 17. Percentage of measurements in a region of the plasma sheet that satisfy the condition $\beta_{xy} > 2$ as a function of the *x* component of the perpendicular flow velocity.

[62] *Data selection*. We use data from the same 17 perigee passes as in section 5, but for this study, since we do not investigate the variations of plasma and field parameters before and after the high-speed flow encounters, we no longer exclude events which occur immediately before or after a lobe encounter. Thus the total number of high-speed ($|\mathbf{v}| > 250$ km/s) bulk flow and field-aligned beam plasma measurements (560 samples) contained in the present statistical survey is larger than that of section 5 (397 samples). The present event selection procedure is purely moment based and does not involve the inspection of individual ion distributions.

[63] *Restricting* β. Figure 18 shows the occurrence of high-speed (>250 km/s) bulk flows as a function of y_{GSM}, restricting to data samples that satisfy $\beta > 2$ condition. Panel a shows the unnormalized distribution. A strong dawn–dusk asymmetry is present, with most events occurring on the dusk ($y_{GSM} > 0$) side. Panel b shows all Wind plasma sheet measurements (irrespective of flow speeds) in the $\beta > 2$ region. The Wind coverage shows no dawn–dusk asymmetry in this region. As a result, the normalized distribution (Panel c) shows a strong asymmetry. Panel d shows the normalized distribution for the $\beta > 0.5$ condition. The dawn–dusk asymmetry in this larger region of the plasma sheet is no longer present.

[64] The complete analysis of the dependence of the dawn–dusk asymmetry on the section criteria based on β is shown in Figure 19a. When there is no restriction on β, i.e., all plasma sheet samples are included, the fast flows (which include field-aligned beams as well) show no dawn–dusk asymmetry. As we confine the plasma sheet region to a smaller and smaller region around the neutral sheet (by increasing the minimum β value), the ratio of dusk

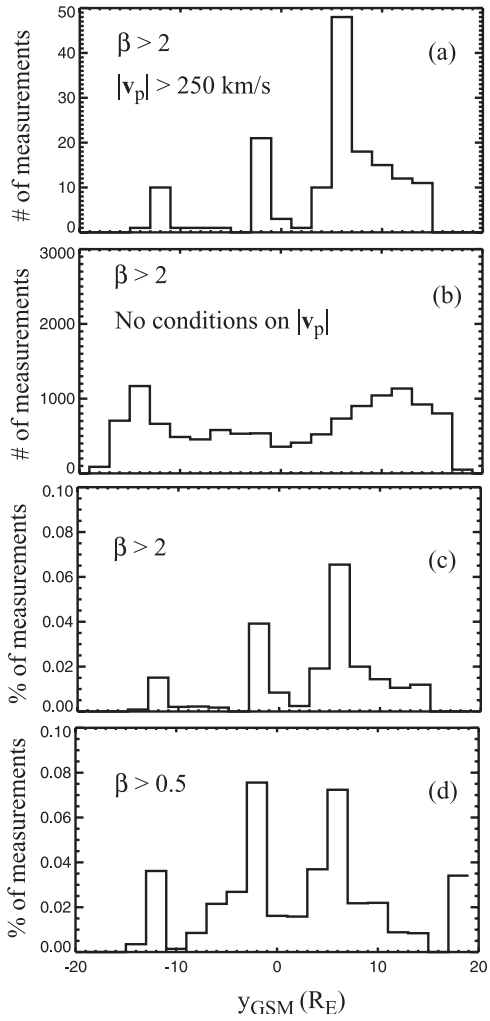

Figure 18. (a) Distribution of high-speed ($|\mathbf{v}| > 250$ km/s) flow measurements that satisfy the $\beta > 2$ as a function of the GSM *y*. (b) Distribution of all plasma sheet (irrespective of flow speed) measurements that satisfy the $\beta > 2$. (c) Normalized distribution of high-speed flows in the $\beta > 2$ region. These mostly bulk flows occur preferentially on the dusk side. (d) Similar to (c), but for $\beta > 0.5$ condition. The dawn–dusk asymmetry is no longer apparent with this selection criterion.

fast flows to dawn fast flows increases, reaching a ratio of 2 to 1 for the $\beta > 2$ condition.

[65] *Restricting* $|B_x|$. The dependence of the dawn–dusk asymmetry on $|B_x|$ is shown in Figure 19b. The trend is similar to that for β. With no restriction on $|B_x|$, the occurrence of fast flows is symmetric about midnight. As $|B_x|$ is restricted to smaller and smaller values, the preference for high-speed flows to occur on the dusk side plasma sheet becomes much more apparent.

[66] *Restricting* $|z_{ns}|$. The dependence of the dawn–dusk asymmetry on the theoretical distance from the neutral sheet, z_{ns}, is shown in Figure 19c. Similar to β and $|B_x|$, the preference for high-speed bulk flows to occur on the dusk side is significant when the region is restricted to $|z_{ns}| < 2\ R_E$.

[67] *Restricting* $v_\perp$. Figure 19d shows that a similar trend when restricting the database on its perpendicular flow speed. The ratio of the number of dusk to dawn events increases with increasing the minimum $v_\perp$ threshold. If one selects only cases with $v_\perp > 300$ km/s, the ratio is 4. This finding is somewhat similar to that found by *Nagai and Machida* [1998] who selected bulk flow events based on $v_{\perp,x} > 300$ km/s.

[68] *Summary*. The above analyses based on β, $|B_x|$, $|z_{ns}|$, and $v_\perp$ produce similar results. The presence of a dawn–dusk asymmetry depends strongly on the selection criteria. Using threshold values of $\beta > 2$, $|B_x| < 5$ nT, $|z_{ns}| < 2\ R_E$, or $v_\perp > 300$ km/s, all of which ensure that great majority of the high-speed flow samples are bulk flows rather than field-aligned beams, a strong dawn–dusk asymmetry in the occurrence of high-speed flows is obtained. If, however, one relaxes these conditions to include a thicker plasma sheet (by increasing the threshold for $|B_x|$ or decreasing the threshold for β and $v_\perp$), the asymmetry becomes weaker and eventually goes away when no restriction on any of these parameters is imposed, i.e., when all plasma sheet regions are considered. These results can be understood as follows: If bulk flows do have a genuine dawn–dusk asymmetry while field-aligned beams do not, the true spatial asymmetry of bulk flows occurrence would emerge only when the event selection criteria imposed assure the inclusion of only bulk flows.

7. Summary

[69] We have surveyed all high-speed (>250 km/s) flows detected by Wind during 17 perigee passes across the near-

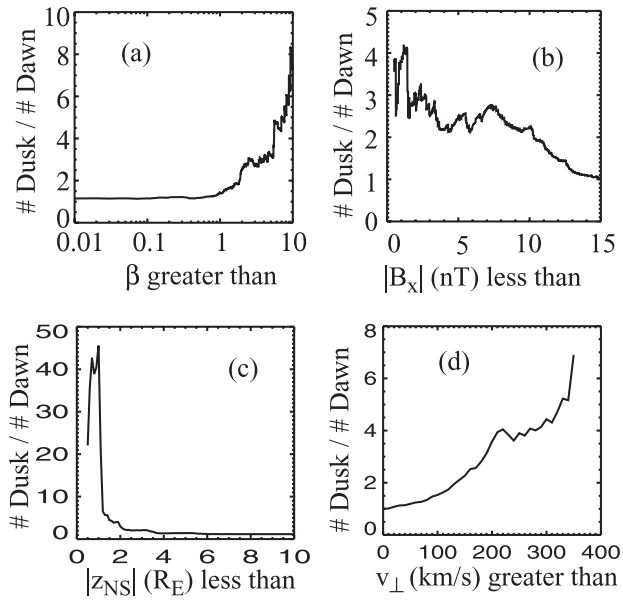

Figure 19. The ratio of dusk to dawn high-speed flow samples (normalized to plasma sheet measurements irrespective of flow speeds) as a function of (a) minimum β, (b) maximum $|B_x|$, (c) maximum $|z_{NS}|$, minimum $v_\perp$. The tendency for high-speed flows to occur on the dusk side is apparent when the data are restricted to large values of β or small values of $|B_x|$, $|z_{NS}|$, and $v_\perp$. These conditions correspond to restricting the data to the plasma sheet region closest to the neutral sheet.

Earth plasma sheet. Based on visual inspection of each ion distribution in high-speed flows, we found that most (if not all) distributions fall into two distinct categories: Bulk flows and field-aligned beams. By classifying high-speed flows based on their ion distribution characteristics, not by criteria based on plasma moments nor by regions where these flows were detected, we examined on an event by event basis the properties of field-aligned beams and bursty bulk flows. Using our classification we also evaluated previously used moment-based selection criteria for differentiating field-aligned beams from convective bulk flows. Below we summarize our main findings.

1. We have demonstrated that the field-aligned beams and bursty bulk flows observed in the near-Earth plasma sheet are distinct.

Bursty bulk flows are characterized by bulk motion of a single population whose core speed is well represented by the velocity moments. Occasionally the Wind spacecraft also detected bulk flow events where a second, colder distribution is present whose $\mathbf{E} \times \mathbf{B}$ drift speed is the same as the dominant distribution but whose parallel velocity is usually much smaller. The velocity moments for these two-population distributions are dominated by the bulk motion of the hotter population. The relative angle between the bulk flow and the magnetic field depends simply on the magnetic field elevation angle. When detected near the neutral sheet, the flows are almost purely convective. At higher magnetic latitudes the bulk flows are more field aligned. Our findings are in close agreement with most of the previous studies of bursty bulk flows [e.g., *Nakamura et al.*, 1991; *Angelopoulos et al.*, 1992; *Nagai et al.*, 1998].

Field-aligned beam ion distributions are easily distinguishable from those of bursty bulk flows. Beam distributions consist of a single earthward crescent-shaped beam or counterstreaming beams having low-energy cutoffs. Bulk flows, on the other hand, are single drifting distributions, irrespective of whether their motions are parallel or perpendicular to the magnetic field. We have classified high-speed flows in the Wind data set into bulk flow and beam categories based on this dramatic difference in their ion distributions.

Bulk flows have the highest occurrence frequency near the neutral sheet ($B_x \sim 0$), but are still detected out to $|B_x| \sim$ 25 nT, while beam events occur primarily away from the neutral sheet, but some events have been detected rather close to the neutral sheet (down to $|B_x| \sim 5$ nT), although none occurred in the neutral sheet itself. Thus, a significant overlapping region (in terms of B_x, β, or Z_{ns} parameters) exists where both types of flows are seen. We have examined the question of whether beams and bulk flows are the same phenomenon viewed at different magnetic latitudes in the plasma sheet. We did not find a case in which beams evolved into bulk flows as the spacecraft traversed the plasma sheet from the lobe toward the neutral sheet. Instead, high-latitude beams always evolve into isotropic and stagnant populations at lower magnetic latitudes.

2. Beams are not associated with changes in the magnetic field. Bulk flows are always accompanied by large fluctuations of the magnetic field and are usually associated with field dipolarization [see also *Angelopoulos*, 1996; *Angelopoulos et al.*, 1992; *Nagai et al.*, 1998; *Fairfield et al.*, 1999]. But on a case by case basis, some bursty bulk flows have been found not to be accompanied by field dipolarization.

3. Field-aligned beams are not associated with changes in the plasma temperature. Bulk flows are often (but not always) associated with temperature enhancements. If the spacecraft initially resides near the neutral sheet, it generally detects little temperature enhancements associated with the arrival of bulk flows. Our finding thus indicates that at least part of the observed temperature increase in conjunction with bulk flow detection is a spatial effect instead of true heating of the plasma.

4. Bulk flows are generally accompanied by sudden enhancements of energetic (up of 0.5 MeV) ion and electron fluxes. Field-aligned beams are not.

5. In agreement with the findings of previous studies [e.g., *Angelopoulos et al.*, 1994; *Nagai and Machida*, 1998], essentially all high-speed bulk flows detected earthward of $x_{GSE} = -17\ R_E$ are directed sunward, indicating that the source region of these flows are generally located tailward of $x_{GSE} = -17\ R_E$.

6. No single parameter—β, β_{xy}, $v_{\perp,x}$, $v_\perp$, or B_x—and threshold can serve to separate beam from bulk flow distributions because a range of values of these parameters exist where both types of flows are detected. We have used our categorization of bulk flow and field-aligned beam events (based on the visual inspection of individual ion distributions) to search for the optimal selection criteria to distinguish bulk flows from beams. We found that with the $\beta > 0.5$ selection criterion, 95% of bulk flow samples are included but at the same time, 55% of undesired beam measurements also satisfies this criterion. The $\beta > 2$ condition, on the other hand, eliminates more than 95% of beam samples and includes 45% of bulk flow samples. The use of $\beta_{xy} > 2$ or $v_\perp >$ 250 km/s conditions are optimal for bulk flow selection since they ensure minimal (less than 5%) beam contamination while retaining ~60% of bulk flow samples.

7. Our survey confirms a dawn–dusk asymmetry reported by *Nagai and Machida* [1998] of the occurrence of earthward bursty bulk flows, with most events occurring in the premidnight sector. In the Nagai and Machida study, tailward convective bulk flows cases also occur preferentially in the premidnight sector. This, and the fact that earthward bursty bulk flows are not directed duskward (Figure 11), imply that the dawn–dusk asymmetry does not arise simply from ion drift toward dusk as they convect earthward. It is however difficult to understand why reconnection, which presumably produces high-speed bulk flows [*Nagai et al.*, 2001], should be initiated preferentially on one side of the magnetosphere. This feature has not been predicted by any existing near-Earth neutral line models.

[70] If one interprets field-aligned beams as signatures of distant-tail reconnection, the absence of a dawn–dusk asymmetry for beams implies that distant-tail reconnection sites have no dawn–dusk bias.

8. Concluding Remarks

[71] While we have demonstrated in this study that bulk flows and beams are distinct phenomena, we have not addressed their sources nor their effects on ionospheric dynamics. To conclusively identify their source regions and mechanisms requires simultaneous multipoint observa-

tions of the magnetotail from near-Earth plasma sheet to the distant tail. For example, to confirm whether field-aligned beams are generated at a distant-tail reconnection site requires simultaneous in situ detection of such a reconnection site. The temporal/spatial nature of fast flows also needs to be investigated with multipoint measurements which could reveal the intrinsic properties of the mechanisms that generate these flows.

[72] In terms of the association of fast flows with substorms, several studies have suggested a close relationship between bulk flows and substorms [e.g., *Nagai et al.*, 1998]. It remains unclear whether bulk flows with and without field dipolarization/plasma heating have different effects. The exact role of field-aligned beams on substorms is also unknown.

[73] Finally, the role of high-speed bulk flows in the overall transport of energy into the inner magnetosphere, which has been a subject of controversies, should be reexamined using a large data set and with our proposed bulk flow event selection criteria (e.g., $\beta_{xy} > 2$).

[74] **Acknowledgments.** We would like to thank Ron Lepping, the principal investigator of the Wind magnetic field experiment, for making his data available. We also thank both referees for their constructive comments and suggestions. This research was funded in part by NASA grant FDNAG5-6928 at University of California at Berkeley.

References

Angelopoulos, V., The role of impulsive particle acceleration in magnetotail circulation, in *Third International Conference on Substorms (ICS-3)*, *ESA SP-389*, pp. 17–22, Eur. Space Agency, Paris, 1996.

Angelopoulos, V., W. Baumjohann, C. F. Kennel, F. V. Coroniti, M. G. Kivelson, R. Pellat, R. J. Walker, H. Luehr, and G. Paschmann, Bursty bulk flows in the inner central plasma sheet, *J. Geophys. Res.*, *97*, 4027, 1992.

Angelopoulos, V., et al., Statistical characteristics of bursty bulk flow events, *J. Geophys. Res.*, *99*, 21,257, 1994.

Angelopoulos, V., F. S. Mozer, R. P. Lin, T. Mukai, K. Tsuruda, R. Lepping, and W. Baumjohann, Comment on "Geotail survey of ion flow in the plasma sheet: Observations between 10 and 50 R_E" by W. R. Paterson et al., *J. Geophys. Res.*, *104*, 17,521, 1999.

Baumjohann, W., G. Paschmann, and C. A. Cattell, Average plasma properties in the central plasma sheet, *J. Geophys. Res.*, *94*, 6597, 1989.

Baumjohann, W., G. Paschmann, and H. Luehr, Characteristics of high-speed ion flows in the plasma sheet, *J. Geophys. Res.*, *95*, 3801, 1990.

Baumjohann, W., G. Paschmann, T. Nagai, and H. Luehr, Superposed epoch analysis of the substorm plasma sheet, *J. Geophys. Res.*, *96*, 11,605, 1991.

Cattell, C. A., and F. S. Mozer, Substorm electric fields in the Earth's magnetotail, in *Magnetic Reconnection in Space and Laboratory Plasmas*, *Geophys. Monogr. Ser.*, vol. 30, edited by E. W. Hones Jr., pp. 208–215, AGU, Washington, D. C., 1984.

Chen, L.-J., G. K. Parks, M. McCarthy, D. Larson, and R. P. Lin, Kinetic properties of bursty bulk flow events, *Geophys. Res. Lett.*, *27*, 1847, 2000.

DeCoster, R. J., and L. A. Frank, Observations pertaining to the dynamics of the plasma sheet, *J. Geophys. Res.*, *84*, 5099, 1979.

Eastman, T. E., L. A. Frank, and C. Y. Huang, The boundary layers as the primary transport regions of the Earth's magnetotail, *J. Geophys. Res.*, *90*, 9541, 1985.

Fairfield, D. H., A statistical determination of the shape and position of the geomagnetic neutral sheet, *J. Geophys. Res.*, *85*, 775, 1980.

Fairfield, D. H., et al., Earthward flow bursts in the inner magnetotail and their relation to auroral brightenings, AKR intensifications, geosynchronous particle injections and magnetic activity, *J. Geophys. Res.*, *104*, 355, 1999.

Forbes, T. G., E. W. Hones Jr., S. J. Bame, J .R. Asbridge, G. Paschmann, N. Sckopke, and C. T. Russell, Evidence for the tailward retreat of a magnetic neutral line in the magnetotail during substorm recovery, *Geophys. Res. Lett.*, *8*, 261, 1981.

Frank, L. A., W. R. Paterson, K. L. Ackerson, S. Kokubun, and T. Yamamoto, Plasma velocity distributions in the near-Earth plasma sheet: A first look with the Geotail spacecraft, *J. Geophys. Res.*, *101*, 10,627, 1996.

Hones, E. W., Jr., Transient phenomena in the magnetotail and their relation to substorms, *Space Sci. Rev.*, *23*, 393, 1979.

Huang, C. Y., L. A. Frank, and T. E. Eastman, Plasma flows near the neutral sheet of the magnetotail, in *Magnetotail Physics*, edited by A. T. Lui, p. 127, Johns Hopkins Univ. Press, Baltimore, Md., 1987.

Lepping, R. P., et al., The Wind magnetic field investigation, *Space Sci. Rev.*, *71*, 207–229, 1995.

Lin, R. P., et al., A three-dimensional plasma and energetic particle investigation for the Wind spacecraft, *Space Sci. Rev.*, *71*, 125–153, 1995.

Lui, A. T. Y., E. W. Hones Jr., F. Yasuhara, S.-I. Akasofu, and S. J. Bame, Magnetotail plasma flow during plasma sheet expansions: VELA 5 and 6 and IMP 6 observations, *J. Geophys. Res.*, *82*, 1235, 1977.

Lui, A. T. Y., T. E. Eastman, D. J. Williams, and L. A. Frank, Observations of ion streaming during substorms, *J. Geophys. Res.*, *88*, 7753, 1983.

Lui, A. T. Y., W. Baumjohann, and G. Rostoker, Substorm expansion onset mechanism debated, *Eos Trans. AGU*, *81*, 70, 2000.

Nagai, T., and S. Machida, Magnetic reconnection in the near-Earth magnetotail, *New Perspectives on the Earth's Magnetotail*, *Geophys. Monogr. Ser.*, 105, edited by A. Nishida et al., pp. 211–224, AGU, Washington, D. C., 1998.

Nagai, T., M. Fujimoto, Y. Saito, S. Machida, T. Terasawa, R. Nakamura, T. Yamamoto, T. Mukai, A. Nishida, and S. Kokubun, Structure and dynamics of magnetic reconnection for substorm onsets with Geotail observations, *J. Geophys. Res.*, *103*, 4419, 1998.

Nagai, T., I. Shinohara, M. Fujimoto, M. Hoshino, Y. Saito, S. Machida, and T. Mukai, Geotail observations of the Hall current system: Evidence of magnetic reconnection in the magnetotail, *J. Geophys. Res.*, *106*, 25,929–25,949, 2001.

Nakamura, M., G. Paschmann, W. Baumjohann, and N. Sckopke, Ion distributions and flows in and near the neutral sheet, *J. Geophys. Res.*, *96*, 5631, 1991.

Nakamura, M., G. Paschmann, W. Baumjohann, and N. Sckopke, Ion distributions and flows in and near the plasma sheet boundary layer, *J. Geophys. Res.*, *97*, 1449, 1992.

Nakamura, R., et al., Substorm observations in the early morning sector with Equator-S and Geotail, *Ann. Geophys.*, *17*, 1602–1610, 1999.

Nishida, A., H. Hayakawa, and E. W. Hones Jr., Observed signatures of reconnection in the magnetotail, *J. Geophys. Res.*, *86*, 1422, 1981.

Onsager, T. G., M. F. Thomsen, R. C. Elphic, and J. T. Gosling, Model of electron and ion distributions in the plasma sheet boundary layer, *J. Geophys. Res.*, *96*, 20,999, 1991.

Parks, G., et al., New observations of ion beams in the plasma sheet boundary layer, *Geophys. Res. Lett.*, *25*, 3285, 1998.

Paterson, W. R., L. A. Frank, S. Kokubun, and T. Yamamoto, Geotail survey of ion flow in the plasma sheet: Observations between 10 and 50 R_E, *J. Geophys. Res.*, *103*, 11,811, 1998.

Petrukovich, A. A., W. Baumjohann, R. Nakamura, R. Schoedel, and T. Mukai, Are earthward bursty bulk flows convective or field-aligned?, *J. Geophys. Res.*, *106*, 21,211–21,215, 2001.

Rostoker, G., and T. E. Eastman, A boundary layer model for magnetospheric substorms, *J. Geophys. Res.*, *92*, 12,187, 1987.

Schindler, K., and J. Birn, On the generation of field-aligned plasma flow at the boundary of plasma sheet, *J. Geophys. Res.*, *92*, 95, 1987.

Sergeev, V. A., R. C. Elphic, F. S. Mozer, A. Saint-Marc, and J. A. Sauvaud, A two-satellite study of nightside flux transfer events in the plasma sheet, *Planet. Space Sci.*, *40*, 1551, 1992.

Takahashi, K., and E. W. Hones Jr., ISEE 1 and 2 observations of ion distributions at the plasma sheet-tail lobe boundary, *J. Geophys. Res.*, *93*, 8558, 1988.

V. Angelopoulos, R. P. Lin, T. Phan, and A. Raj, Space Sciences Laboratory, University of California at Berkeley, Centennial Drive at Grizzly Peak Boulevard, Berkeley, CA 94720-7450, USA. (phan@ssl.berkeley.edu)